

## ARTICLE OPEN



# Analysis of factors influencing tropical lower stratospheric water vapor during 1980–2017

Jinpeng Lu<sup>1</sup>, Fei Xie<sup>1</sup>✉, Cheng Sun<sup>1</sup>, Jiali Luo<sup>2</sup>, Qifa Cai<sup>3</sup>, Jiankai Zhang<sup>2</sup>, Juan Li<sup>3</sup> and Hongying Tian<sup>2</sup>

Tropical cold point tropopause temperature (CPT) anomalies determine lower stratospheric water vapor (LSWV) variations, leading to a high correlation between variations in tropical average CPT and changes in tropical average LSWV. However, this high correlation is only found in winter and spring. This work revisits the factors controlling LSWV variations using observations and simulations over the past ~40 years. It is found that the first and second empirical orthogonal function (EOF) modes of tropical CPT variations together explain the tropical average LSWV changes much better than the tropical average CPT variations. The high correlation between the first and second EOF modes of tropical CPT variations and tropical average LSWV changes holds in all four seasons. A further analysis shows that the first and second EOF modes of tropical CPT variations are related to canonical El Niño–Southern Oscillation (ENSO) activity and sea surface temperature (SST) variations in the central Pacific Ocean, respectively. ENSO Modoki is also an important factor that affects LSWV variations by influencing the vertical velocity at the tropopause. The quasi-biennial oscillation (QBO) affects the CPT, and is the third process modulating the LSWV changes. The simulations also support the results.

*npj Climate and Atmospheric Science* (2020)3:35; <https://doi.org/10.1038/s41612-020-00138-7>

## INTRODUCTION

Stratospheric water vapor (SWV) plays an important role in regulating the global radiation budget, energy balance, stratospheric temperature and chemical processes, and global climate change<sup>1–5</sup>. Increases and decreases in SWV have been found to strengthen and offset global warming effects, respectively<sup>6,7</sup>. Therefore, understanding the variations and controlling factors of SWV is important for the prediction of global climate change.

The main source of water vapor in the middle and upper stratosphere is methane oxidation in the stratosphere<sup>8,9</sup>, but in the lower and middle stratosphere the main source is the transport of air through upwelling from the tropical tropopause layer (TTL) into the stratosphere<sup>10,11</sup>. The influence of SWV variations on climate change is mainly caused by the variations in the lower and middle stratosphere<sup>6</sup>. Brewer<sup>12</sup> first showed the large-scale transport of tropospheric air into the stratosphere in the tropics and its dehydration by cold temperatures near the tropical tropopause. Therefore, vertical transport is a factor affecting the variations of water vapor in the lower stratosphere. Tropical lower SWV (LSWV) changes have been an active research topic in recent years. Many studies have investigated LSWV variations and their link with global climate change<sup>13–16</sup>.

It is well known that tropical tropopause temperature is the main factor controlling tropical SWV through dehydration<sup>12,17–26</sup>, as determined by dynamical, radiative, and chemical processes in the TTL<sup>27–29</sup>. The TTL is not just a geometric surface, but is rather a thin layer with spatial structure, and various physical processes in TTL affect water vapor transport through this channel into the stratosphere<sup>11,30,31</sup>. Weakening (strengthening) of the stratospheric Brewer–Dobson (BD) circulation (e.g., Birner and Bönisch<sup>32</sup>) driven by extratropical stratospheric waves increases (decreases) the tropopause temperature<sup>4,5,33–35</sup>. In addition, the temperature of the TTL is also driven by equatorial planetary waves including both tropical Rossby and Kelvin waves. Several

studies have demonstrated that penetrating deep convection systems can contribute to LSWV<sup>28,36–38</sup>. Tropical deep convection cools the upper part of the TTL through wave-induced upward motion near the tropopause<sup>23,39,40</sup>.

As El Niño–Southern Oscillation (ENSO) can influence the tropical upwelling and tropopause temperature<sup>41,42</sup>, it is one of the most important processes controlling LSWV changes on interannual time scales. The enhanced tropical upwelling warms the upper troposphere and cools the lower stratosphere in the tropics during El Niño phases<sup>43–46</sup>, influencing large-scale tropical water vapor concentrations<sup>18,20,47–50</sup>. The vertical propagation of ultralong Rossby waves is intensified during El Niño activity in the Northern Hemisphere (NH) during NH winter. Observational datasets show anomalous increased wave dissipation in the stratosphere in the NH middle and high latitudes, warming the Arctic stratosphere and cooling the equatorial stratosphere<sup>44,51–55</sup>. This is also supported by simulations<sup>43,50,56–61</sup>. La Niña activity has the opposite effect on the middle-latitude and polar stratosphere<sup>44,61–65</sup>.

In recent decades, a change in the ENSO anomaly pattern, referred to as the Central Pacific (CP) ENSO (or ENSO Modoki), which is distinct from the familiar Eastern Pacific (EP) ENSO (canonical ENSO), has gradually become apparent<sup>66,67</sup>. The gradient pattern of sea surface temperature (SST) anomalies (SSTA) of El Niño Modoki leads to a different pattern of propagation and dissipation of ultralong Rossby waves in the middle-latitude stratosphere that can affect the stratosphere, unlike the case for the canonical El Niño. Thus, the climatic effects of ENSO Modoki on stratospheric circulation are different from those of the canonical ENSO<sup>50,63,68–75</sup>. The variations in convection and circulation patterns resulting from SSTAs have been shown to significantly influence tropopause temperatures<sup>76</sup>. Walker circulation patterns and the effects of convection anomalies caused by El Niño Modoki activity can extend to the TTL. Xie et al.<sup>50</sup> found that

<sup>1</sup>Change and Earth System Science, Beijing Normal University, Beijing, China. <sup>2</sup>College of Atmospheric Sciences, Lanzhou University, Lanzhou, China. <sup>3</sup>Mailbox 5111, Beijing, China. ✉email: xiefei@bnu.edu.cn

ENSO Modoki caused changes in the tropopause temperature and SWV anomalies, although the influence of ENSO Modoki is smaller than that of the canonical ENSO. Ding and Fu<sup>77</sup> also presented observational and modeling evidence that the epochal change of water vapor between 1992–2000 and 2001–2005 was also partly caused by a concurrent SST warming in the tropical central Pacific. This SST warming cools the TTL<sup>78</sup> overhead by enhancing equatorial-wave-induced upward motion near the tropopause, which consequently reduces the amount of water vapor entering the stratosphere. Thus, ENSO Modoki is also an important process controlling LSWV changes on interannual time scales.

The quasi-biennial oscillation (QBO) is a downward-propagating oscillating pattern of equatorial stratospheric winds and temperatures with a period of ~2 years. As early as 1964, Reed<sup>79</sup> pointed out the meridional circulation induced by the QBO would produce a QBO signal in total column ozone. The tropopause temperature changes associated with the QBO drive an ~2-year periodicity in water vapor interannual anomalies near the tropical tropopause, and these propagate with the mean stratospheric transport circulation (in a manner similar to the seasonal “tape recorder”) vertically and latitudinally<sup>80</sup>. Geller et al.<sup>48</sup> showed that QBO-induced mean meridional circulation led to the dynamical redistribution of water vapor in the middle and upper stratosphere, and that the dehydration signal accompanying the QBO variation of the tropical cold point tropopause caused the “tape recorder” pattern, which dominated QBO water vapor variability.

During an easterly QBO phase (EQBO), the upwelling anomalies in the lower stratosphere at the equator lead to a negative anomaly in tropopause temperature. As expected from the thermal wind relationship, a descending westerly QBO phase (WQBO), in which warm temperature anomalies near the tropopause are associated with positive (westerly) wind shear, will take 2–3 months to propagate downwards from 50 hPa to the tropopause<sup>81</sup>. Thus, the QBO can affect the upper part of the TTL and act as the primary perturbation of TTL temperature that influences the LSWV on interannual time scales<sup>17,82</sup>. Ding and Fu<sup>77</sup> showed that the influence of the QBO (at 50 hPa) on temperature over 15°S–15°N at 85 hPa and water vapor at 83 hPa in the lower stratosphere were well correlated, and that the QBO (at 50 hPa) affected SWV by influencing the tropopause temperature.

Although there have been many studies investigating the LSWV variations and related mechanisms and drivers, there are still some aspects that require further analysis. For example, it is well known that tropopause temperature is the main factor controlling the variations in LSWV. However, Rosenlof<sup>83</sup> pointed out that vertical transport may also have important effects on LSWV changes. Is it possible to separate the contributions of tropopause temperature and vertical transport intensity near the tropopause to SWV variations? Many studies have investigated the effects of ENSO and the QBO on lower stratospheric water variations. ENSO and the QBO first influence the tropopause temperature or the vertical velocity before affecting water vapor. However, the relationships among ENSO or the QBO (the indirect factors for water vapor changes), tropopause temperature or vertical velocity (the direct factors for water vapor changes), and LSWV changes are not clear. This work investigates these issues using observations, reanalysis, and long-term model data.

## RESULTS

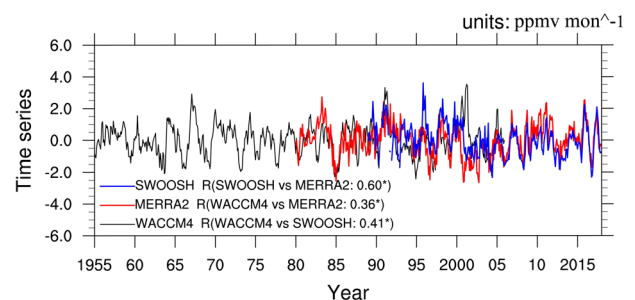
Factors influencing leading mode of tropical LSWV changes

Figure 1 shows monthly time series of water vapor anomalies averaged over 30°S–30°N at 85 hPa with the annual cycle and linear trend removed from the original Modern-Era Retrospective analysis for Research and Applications, Version 2 (MERRA-2) reanalysis data (1980–2017, red line) and Stratospheric Water and Ozone Satellite Homogenized (SWOOSH) data (1984–2017,

blue line). This two time series are highly consistent over their overlapping period (Fig. 1). Although the SWOOSH dataset is a merged dataset of SWV measurements taken by a number of limb sounding and solar occultation satellites, there are still many missing values that can affect an analysis of horizontal variations. Therefore, we use MERRA-2 reanalysis water vapor data in this study.

First, we perform an empirical orthogonal function (EOF) analysis of LSWV anomalies within 30°S–30°N at 85 hPa based on MERRA-2 data for the period 1980–2017 to investigate the characteristics of water vapor variations and possible factors affecting the corresponding leading modes (Fig. 2). The first EOF mode of water vapor (EOF\_WV1) accounts for 47.0% of the variance (Fig. 2a). The correlation coefficient between the first temporal mode of water vapor (PC\_WV1) and the time series of LSWV is 0.96, significant at the 95% confidence level (Fig. 2b), implying that the EOF\_WV1 captures the main characteristics of changes of water vapor in the stratosphere. In agreement with previous studies, the spatial structure of EOF\_WV1 is symmetric about the equator<sup>77</sup>. There are positive water vapor anomalies in the tropical lower stratosphere in the regions 30°S–30°N, 0°–180°E and 30°S–30°N, 120°W–0° (Fig. 2a). Note that the amplitude of water vapor anomalies over 60°E–180° is much larger than over 60°W–0°. As the TTL over the western Pacific Ocean is the main channel through which water vapor enters the stratosphere<sup>19,84</sup>, the amplitude of the water vapor anomalies at 60°E–180° is large. Negative water vapor anomalies are found between 180° and 120°W. The temperature of the tropopause is known to be the main factor controlling tropical SWV through dehydration<sup>11,12,17–19,21–24</sup>. The correlation coefficient between PC\_WV1 and the time series of tropical cold point tropopause temperature (CPT) is 0.70, significant at the 95% confidence level (Fig. 2c).

An EOF analysis of CPT changes within 30°S–30°N for the period 1980–2017 is performed on MERRA-2 data. The temporal first and second principal components of CPT variations are hereafter referred to as PC\_T1 and PC\_T2, respectively. It is interesting that the correlation coefficient between PC\_WV1 and the combination of the first two principal components (PC\_T1 + PC\_T2) based on the combination of the variances is 0.89 (Fig. 3a), which is significant at the 95% confidence level. After analyzing the range of uncertainty in the correlation coefficients, it is found that 0.89 is significantly higher than that between PC\_WV1 and the time series of tropical CPT (0.70; Fig. 2c). The correlation coefficient between (PC\_T1 + PC\_T2) and the tropical LSWV time series is 0.84, significant at the 95% confidence level (Fig. 3b). Figure 3c–f shows scatter plots of LSWV anomalies versus (PC\_T1 + PC\_T2) variations in all four seasons. The correlation coefficients between



**Fig. 1** The time series of water vapor anomalies at 85 hPa from different data. Monthly mean time series of water vapor anomalies at 85 hPa (water vapor anomalies at 85 hPa are an average over 100–70 hPa, here and in later figures) in the tropics (30°S–30°N). For SWOOSH data (1984–2017; blue line), MERRA-2 reanalysis data (1980–2017; red line), and WACCM4 data (1955–2005; black line). Anomalies are obtained by removing the annual cycle and linear trend from the original data. Asterisks indicate that the correlation coefficient (R) is significant at the 95% confidence level.

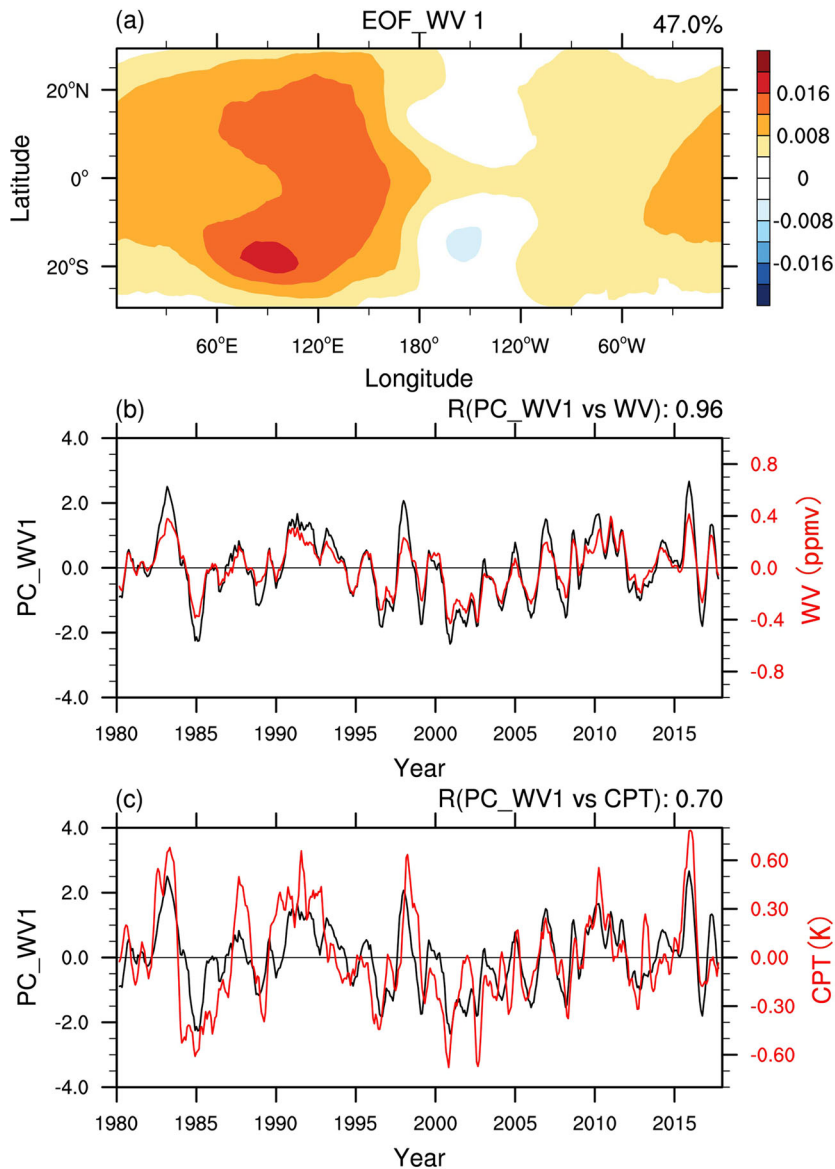


**Fig. 2** The first spatial mode of the EOF analysis of LSWV variations. The first spatial mode of the EOF analysis of LSWV variations is EOF\_WV1 and the temporal mode is PC\_WV1. LSWV variations are at 85 hPa for the period 1980–2017 using MERRA-2 data covering 30°S–30°N. LSWV variations were obtained by removing the annual cycle and linear trend from the original time series at each grid cell. The square-root of the cosine of latitude was used for the weighting function in the EOF analysis. **a** EOF\_WV1. The value in the upper right corner is the explained variance of the mode. **b** PC\_WV1 (black line) and the time series of water vapor anomalies averaged at 85 hPa in the tropics (30°S–30°N; WV; red line). **c** PC\_WV1 (black line) and the time series of CPT anomalies averaged in the tropics (30°S–30°N; CPT; red line). The values in the upper right corner in **b** and **c** are the correlation coefficients.

LSWV anomalies and  $(PC_{T1} + PC_{T2})$  variations in winter, spring, summer, and autumn are 0.86, 0.84, 0.89, and 0.90, respectively. Randel and Jensen<sup>11</sup> have shown that the correlation coefficients between LSWV and tropopause temperature are high only in winter and spring ( $r = 0.89$ ), and are low in summer and autumn ( $r = 0.39$ ). Our results better explain the LSWV variations with CPT. Individual components of the CPT change (like the first and second modes), rather than the total CPT change, have a greater impact on LSWV variations. This suggests that using only the first and second modes of CPT changes may aid investigations of the relationship between CPT and LSWV.

What are the factors affecting the first and second modes of CPT changes? Figure 4a and c shows the first and second spatial modes from the EOF analysis of CPT variability (EOF\_T1 and EOF\_T2). The EOF\_T1 accounts for 32.7% of the variance. The

pattern of EOF\_T1 (Fig. 4a) is similar to the CPT anomalies caused by the canonical ENSO, because convection anomalies during canonical ENSO events influence Rossby wave divergence and tropical upwelling anomalies that further influence the tropopause temperature in the tropics<sup>18,19,47–50,85</sup>. The time series of PC\_T1 and the NINO3.4 index (Fig. 4b) reveals a high correlation ( $r = 0.79$ ). This implies that the canonical ENSO may influence the CPT and thus modulates the LSWV. EOF\_T2 accounts for 19.7% of the variance and has positive temperature anomalies in the region 30°S–30°N and 120°E–120°W (Fig. 4c). Ding and Fu<sup>77</sup> found that SST warming in the tropical central Pacific cools the TTL by enhancing the equatorial-wave-induced upward motion near the tropopause, which consequently reduces the amount of water vapor entering the stratosphere. The pattern evident in Fig. 4c is similar to those of Figs 5, 7, and 8 of Ding and Fu<sup>77</sup>. Thus, there is a

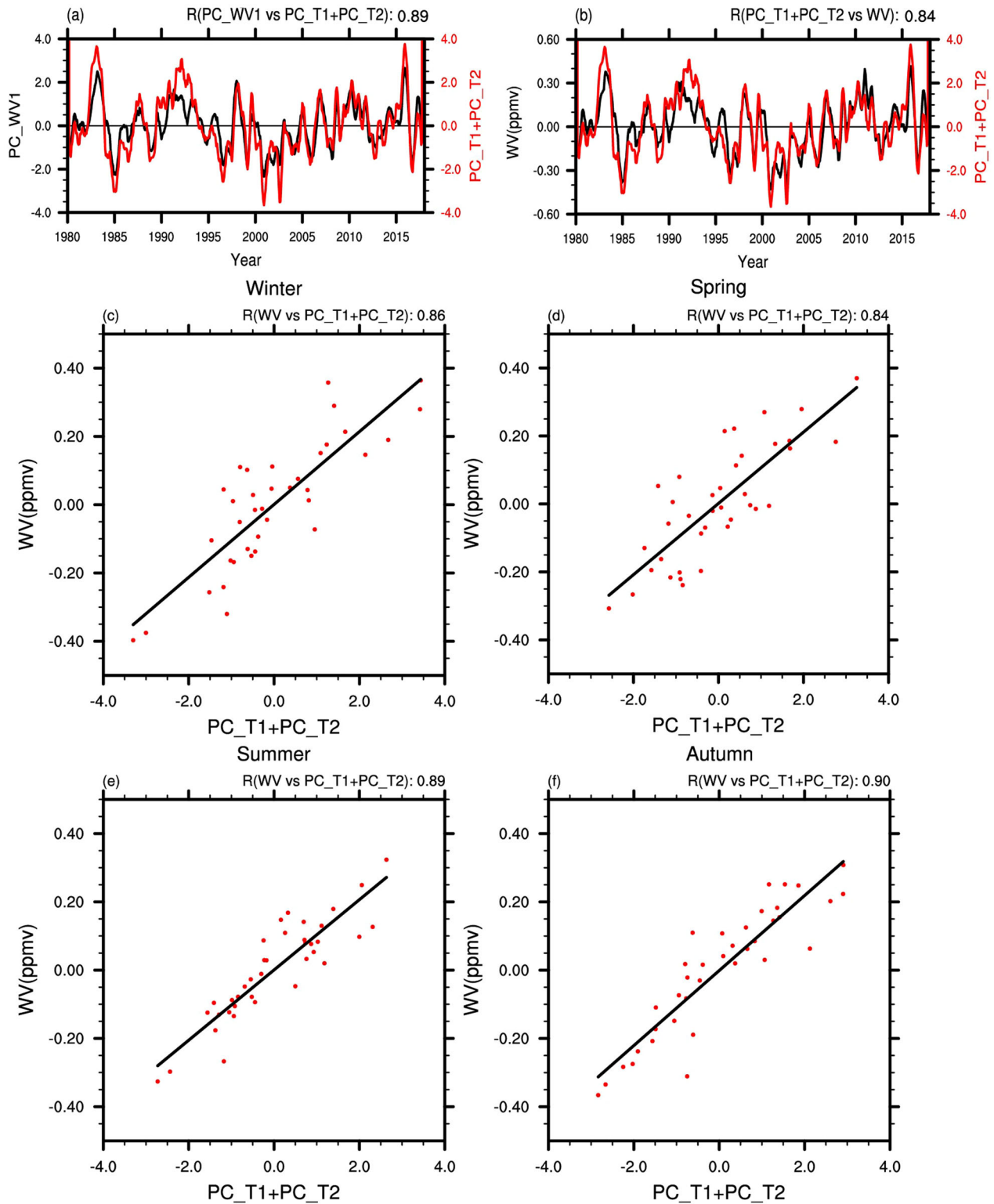


**Fig. 3 LSWV anomalies versus the tropopause temperature variability.** EOF analysis of CPT variability for the period 1980–2017 using MERRA-2 data covering 30°S–30°N. The first, second and third spatial modes from the EOF analysis of CPT variability are EOF\_T1, EOF\_T2, and EOF\_T3, respectively. The first, second, and third temporal modes are PC\_T1, PC\_T2, and PC\_T3, respectively. **a** PC\_WW1 (black line) and (PC\_T1 + PC\_T2; red line). PC\_WW1 is the first temporal mode of LSWV variations as defined in Fig. 2. **b** Time series of average water vapor anomalies in the tropics (30°S–30°N) at 85 hPa (black line) and (PC\_T1 + PC\_T2; red line). Scatter plots of water vapor anomalies at 85 hPa versus (PC\_T1 + PC\_T2) in NH **c** winter, **d** spring, **e** summer, and **f** autumn. The values in the upper right corner are the correlation coefficients.

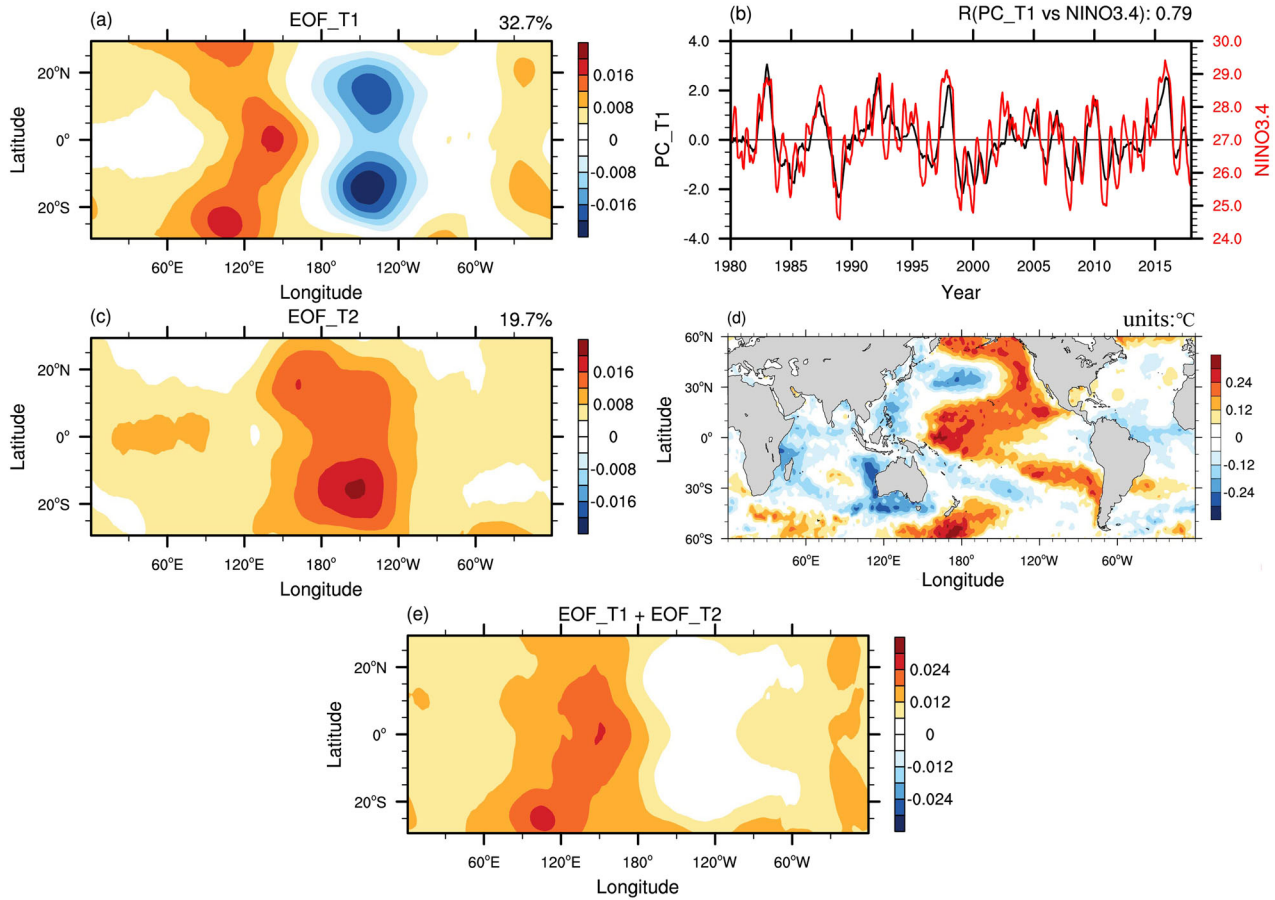


**Fig. 4 Canonical ENSO events and SST in the tropical central Pacific controlling tropopause temperature changes. a** EOF\_T1; **b** PC\_T1 (black line) and the NINO3.4 index (red line); **c** EOF\_T2; **d** Spatial pattern of correlation coefficients between PC\_T2 and SST; and **e** EOF\_T1 + EOF\_T2. Please refer to the caption of Fig. 3 for descriptions of EOF\_T1, EOF\_T2, PC\_T1, and PC\_T2.

good correlation between PC\_T2 and SST in the tropical central Pacific (Fig. 4d). Figure 4d agrees with Fig. 6 of Ding and Fu<sup>77</sup>.

The above analysis shows that the first and second modes of CPT can explain the first mode of tropical LSWV variations (or average tropical LSWV). Figure 4e shows the combination of EOF\_T1 and EOF\_T2. The combined temperature anomalies in the tropics have two positive centers in the regions 0–180°E and 120°W–0°, corresponding closely to the structure of EOF\_WV1 (Fig. 2a). This further indicates a joint effect of the first and second modes of CPT on LSWV variations. Note that although the variance of EOF\_T1 is larger than that of EOF\_T2, EOF\_T1 (Fig. 4a) has a dipole structure with positive and negative centers, whereas EOF\_T2 has only positive anomalies (Fig. 4c). Therefore, EOF\_T2 makes a greater net contribution to SWV variations than does EOF\_T1. This is why Ding and Fu<sup>77</sup> found that the warming of the central Pacific Ocean resulted in a cooling of the tropopause, which is the main cause of drying in the stratosphere.

#### Factors influencing residual modes of tropical LSWV changes

We next analyze the changes of residual LSWV and related controlling factors. Note that for this we do not directly analyze the second and higher modes from the above EOF analysis of LSWV variations (Fig. 2). We first remove the first mode [PC\_WV1, which is related to (PC\_T1 + PC\_T2)] from the LSWV variations by regression. Then, we apply EOF analysis to the residual LSWV variations and investigate the first leading mode of this residual LSWV. This method helps to analyze the key factors without the effects from interference factors. The first mode of the residual LSWV variations (EOF\_R\_WV1) accounts for 49.2% of the variance

of the residual variations (Fig. 5a). It has a tripolar structure—i.e., positive water vapor anomalies in the regions 0°–90°E and 0°–150°W, and negative anomalies at 90°E–150°W. Figure 5b shows the first temporal mode of residual LSWV variations (PC\_R\_WV1) and the EMI (the definition of EMI please see “Data and model” section) for the period 1980–2017. The correlation coefficient between PC\_R\_WV1 and EMI is 0.51, significant at the 95% confidence level (Fig. 5b). This suggests that the first mode of residual LSWV variations may be related to ENSO Modoki events. Figure 5c shows the composite CPT anomalies according to the EMI. There are positive temperature anomalies in the regions 0°–120°W and 60°E–120°E, and negative anomalies at 120°E–120°W (Fig. 5c). This agrees with the results of Xie et al.<sup>50</sup>. However, the locations of the negative centers in Fig. 5c are not the same as in Fig. 5a suggesting that the CPT anomalies related to ENSO Modoki events may not be the main cause of the first mode of residual LSWV variations.

As pointed out by previous studies (e.g., Rosenlof<sup>83</sup>), the variations of water vapor in the lower stratosphere are affected by tropopause temperature as well as by the strength of vertical transport—i.e., stronger upwelling transports more water vapor into the stratosphere. We use the vertical velocity anomalies in the tropopause to represent the strength of vertical transport in this study. The vertical velocity variations are highly correlated with the EMI in the region 30°S–30°N and 120°E–150°W (Fig. 5d,  $r = 0.58$ ), where water vapor anomalies reach their maxima in Fig. 5a. Figure 5e shows the composite water vapor anomalies at 85 hPa may be related to the vertical velocity variations. Similar to Fig. 5a, there is a tripolar structure—i.e., positive water vapor anomalies in

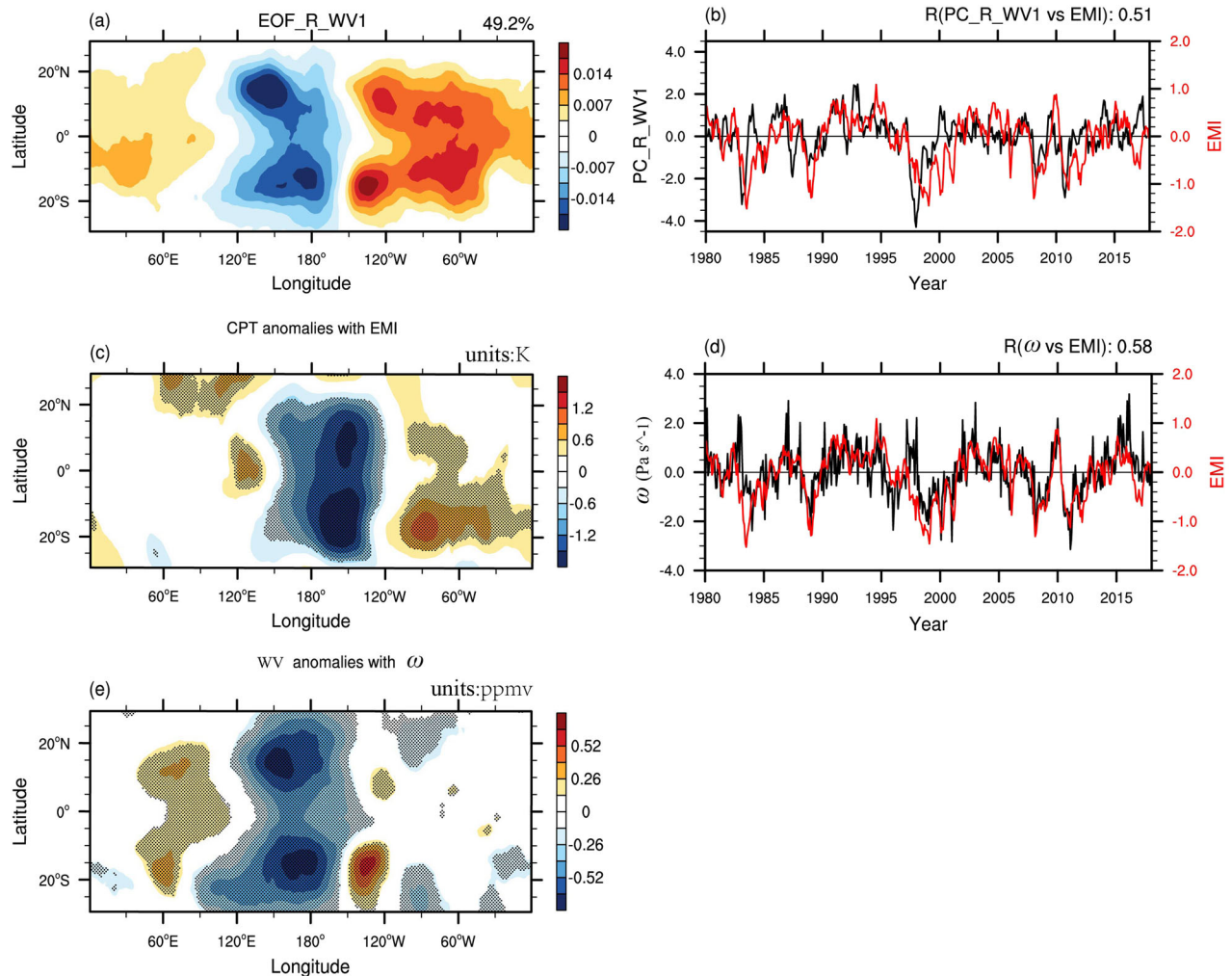


**Fig. 5** The impact of ENSO Modoki on the LSWV variations by vertical transport. EOF analysis of residual LSWV variations at 85 hPa for the period 1980–2017 using MERRA-2 data covering 30°S–30°N. The spatial mode of the first EOF mode is EOF\_R\_WV1 and its temporal mode is PC\_R\_WV1. Residual LSWV variations are obtained by removing PC\_WV1 from LSWV variations by regression. **a** EOF\_R\_WV1; **b** PC\_R\_WV1 (black line) and the EMI (red line); **c** Composite CPT anomalies from MERRA-2 data between positive and negative ENSO Modoki events for the period of 1980–2017 based on the EMI; **d** 150 hPa vertical velocity variations ( $\omega$  (omega), black line) and the EMI (red line);  $\omega$  (omega) variations are averaged in the region 30°S–30°N and 120°E–150°W; and **e** Composite 85 hPa water vapor anomalies from MERRA-2 data between positive and negative  $\omega$  (omega) events for 1980–2017 based on the  $\omega$  (omega) variations in **d**. A positive (negative) standard deviation of EMI and  $\omega$  (omega) variations is used as a threshold to select positive (negative) events. Details of selected events are not shown.

the regions 90°E–150°E and 0°–150°W, and negative anomalies at 150°E–150°W (Fig. 5e). The locations of negative centers in Fig. 5e are in good agreement with those of Fig. 5a, implying that the first mode of residual LSWV variations may be related to vertical velocity anomalies associated with ENSO Modoki events.

We next analyze the changes of residual LSWV after removing both PC\_WV1 and PC\_R\_WV1 from LSWV changes by regression. The first spatial mode of residual LSWV changes is EOF\_RR\_WV1, which accounts for 49.6% of the variance and has a symmetric banded structure across the equator (Fig. 6a)—i.e., negative water vapor anomalies in 15°S–15°N and positive anomalies in 15°S–30°S and 15°N–30°N. The first temporal mode of these residual LSWV changes (PC\_RR\_WV1) is significantly correlated with the third mode of CPT changes (Fig. 6b, PC\_T3,  $r = 0.68$ ). This suggests that the third mode of CPT variations also affects the SWV changes. The spatial structure of the third mode of CPT changes (EOF\_T3, accounting for 7.8% of the variance, Fig. 6c) is consistent with EOF\_RR\_WV1 (Fig. 6a), which also has a symmetric banded structure across the equator. It is well known that the QBO can affect tropopause temperature. The PC\_T3 has a quasi-2-year cycle

(Fig. 6b) and the correlation coefficient between the QBO index and PC\_T3 is 0.65 (Fig. 6d). EOF\_T3 also has symmetric positive and negative phases (Fig. 6c). Thus, the net impact of the third mode of CPT, which is related to the QBO, on the SWV is weak. As EOF\_WV1, EOF\_R\_WV1, and EOF\_RR\_WV1 explain nearly 80% of the variance (47.0% for EOF\_WV1, (49.2% of 16.9%) of EOF\_R\_WV1 and (49.6% of 5.5%) of EOF\_RR\_WV1) of tropical SWV variation, the changes of other modes of residual LSWV will not be analyzed further.

#### Supported by simulation

The SWV variations from version 4 of the Whole Atmosphere Community Climate Model (WACCM4) data are consistent with those from SWOOSH data during the overlapping time period (Fig. 1). Thus, the WACCM4 data for the longer period (1955–2005) are used to perform the same analysis to confirm the results of MERRA-2. Figure 7 shows the characteristics of water vapor variations of the corresponding leading modes within 30°S–30°N at 85 hPa based on WACCM4 data for 1955–2005 and possible drivers. Using the same methods as for MERRA-2 data, we

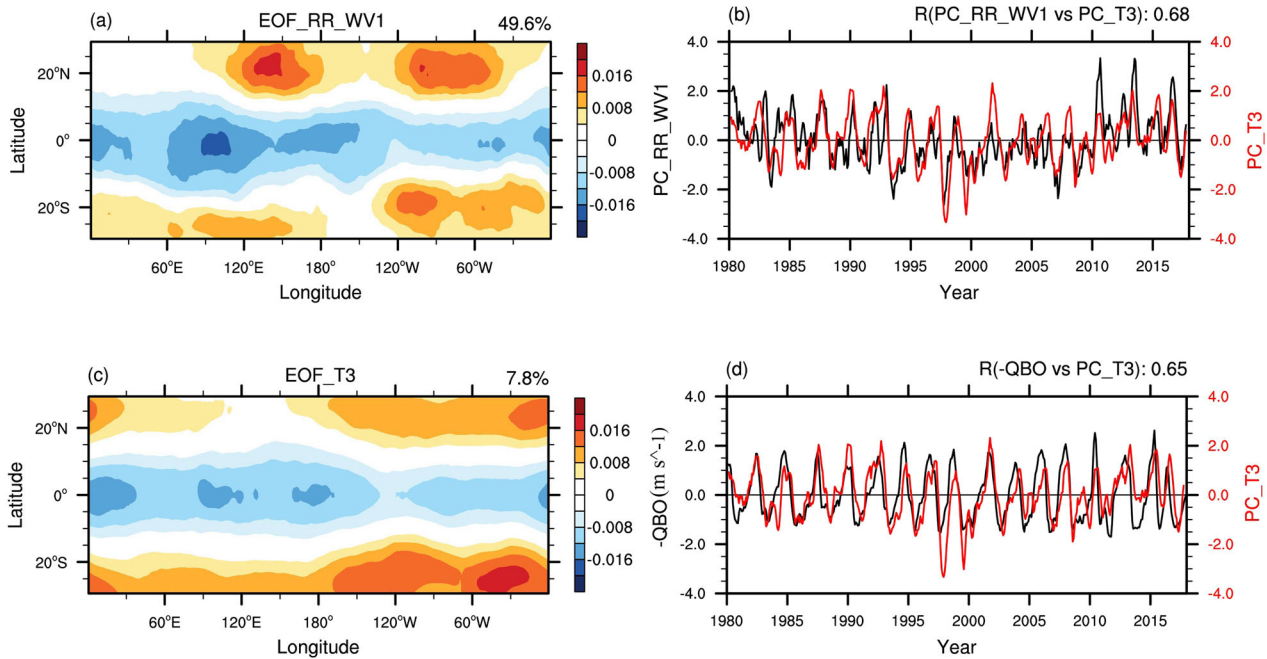


**Fig. 6** The impact of QBO on the LSWV variations. EOF analysis of residual LSWV variations at 85 hPa for the period 1980–2017 using MERRA-2 data covering 30°S–30°N. The spatial mode of the first EOF mode is EOF\_RR\_WV1 and the temporal mode is PC\_RR\_WV1. The residual LSWV variations used here are obtained by removing PC\_WV1 and PC\_R\_WV1 from LSWV variations by regression. **a** EOF\_RR\_WV1; **b** PC\_RR\_WV1 (black line) and PC\_T3 (red line); **c** EOF\_T3; and **d** 50 hPa QBO index (inverted for ease of comparison) (black line) and PC\_T3 (red line). PC\_T3 is defined in the caption of Fig. 3.

obtained EOF\_WV1 (Fig. 7a), EOF\_R\_WV1 (Fig. 7c), and EOF\_RR\_WV1 (Fig. 7e) from WACCM4 data. Their spatial structures are similar to those from MERRA-2 (Figs 2a, 5a, and 6a). The explained variances of EOF\_WV1, EOF\_R\_WV1, and EOF\_RR\_WV1 from WACCM4 data are 75.3%, 76.1%, and 69.3%, somewhat larger than in Figs 2a, 5a, and 6a. The correlation coefficient between PC\_WV1 and (PC\_T1 + PC\_T2) is 0.58, significant at the 95% confidence level (Fig. 7b). The correlation coefficient between PC\_R\_WV1 and EMI reaches 0.44 (Fig. 7d). PC\_RR\_WV1 is also correlated with the third mode of tropopause temperature changes (PC\_T3,  $r = 0.36$ ). Results of the simulation support the conclusions reached using MERRA-2 data.

## DISCUSSION

We investigated factors affecting LSWV variations from 1980 to 2017 using MERRA-2 reanalysis data and from 1955 to 2005 with WACCM4 simulation data, and identified mechanisms affecting water vapor in the lower stratosphere. The most important direct factors affecting the first mode of LSWV changes from 1980 to 2017 are the first and second modes of CPT changes, and the corresponding indirect drivers are the canonical ENSO (EP ENSO) activity and the variations of SST in the central Pacific Ocean. The second most important direct process affecting LSWV changes from 1980 to 2017 may be related to the change in vertical velocity near the tropopause, and the corresponding indirect driver is ENSO Modoki (CP ENSO) activity. The third mode of CPT changes also have a direct influence on water vapor changes in the lower stratosphere, and this direct factor is related to the QBO. Results suggest that the canonical ENSO, SST in the central Pacific Ocean, and the QBO can affect the CPT and thus influence the LSWV. However, ENSO Modoki influences the LSWV may be related to vertical velocity near the tropopause.

Here we discuss why the two types of ENSO affect SWV through different mechanisms. ENSO events can influence tropopause temperature and vertical velocity. The main mode of tropopause

temperature variations is related to changes in equatorial planetary waves including tropical Rossby and Kelvin waves in response to ENSO<sup>23,39,86</sup>. ENSO influences the deep convection that further affects vertical velocity near the tropopause<sup>87</sup>. Xie et al.<sup>50</sup> showed that the tropopause temperature responses to the canonical ENSO are stronger than those to ENSO Modoki. However, Xie et al.<sup>88</sup> showed that the impact of ENSO Modoki events on deep convection is stronger than that of the canonical ENSO. This may explain why the canonical ENSO influences SWV via tropopause temperature but ENSO Modoki influences SWV via vertical transport.

Another issue worth discussing is that ENSO Modoki influences the variations of the SST in the central Pacific Ocean, it is hard to separate the effects of SST anomalies in the central Pacific Ocean and ENSO Modoki events on stratosphere. Note that the index of SST in the central Pacific is somewhat different from the EMI, and the pattern of SST anomalies in the central Pacific is also different from that of ENSO Modoki. Ding and Fu<sup>77</sup> showed that SST in the central Pacific Ocean influences upwelling due to the modulation of wave activity, which further influences tropopause temperature and water vapor. However, Xie et al.<sup>88</sup> found that ENSO Modoki influences deep convection and further affects water vapor. This may be the different pathways or mechanisms by which the two linked patterns of the Central Pacific Ocean SST anomalies affecting the stratosphere. But it is indeed a more complex issue that needs further discussion and study in future work.

## METHODS

### Linear regression analysis

Linear regression analysis is on the basis of the assumption that the controlling factors are orthogonal to each other, and directly subtracting the signal obtained by the regression from raw time series can remove the signal in the LSWV variations. Removing other signals from the LSWV variations by regression, it reduces the influences from other signals when investigating the main signal in the LSWV variations. This method helps to analyze the key factors without the effects from interference factors.

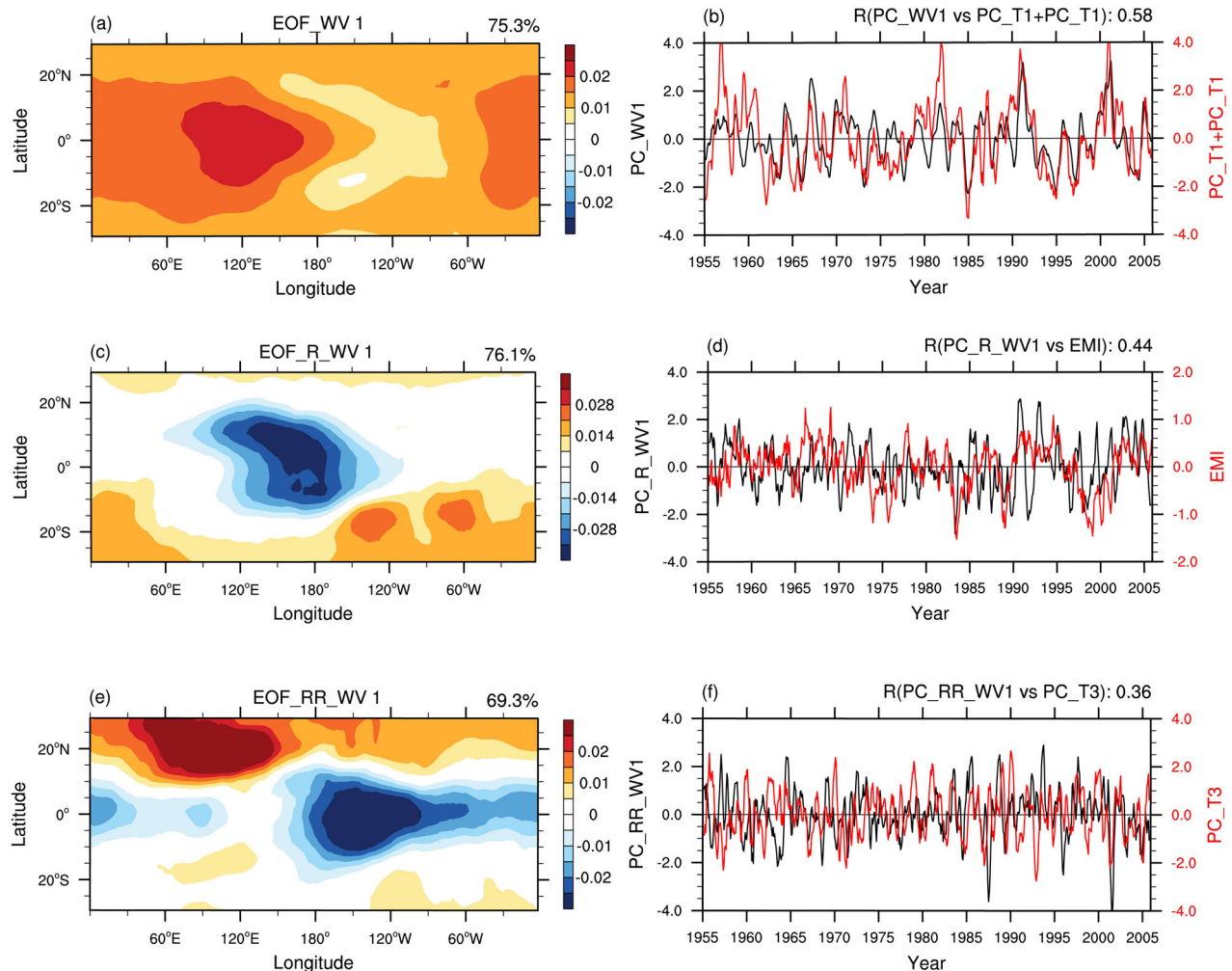


**Fig. 7** EOF analysis of LSWV variations from WACCM4 data. **a, b** As in Figs 2a and 3a, **c, d** as in Fig. 5a, b, and **e, f** as in Fig. 6a, b, but for results of the EOF analysis and correlation obtained from WACCM4 water vapor. The WACCM4 water vapor covering 30°S–30°N at 85 hPa for the period of 1955–2005.

## Data

Monthly water vapor data are taken from the Stratospheric Water and Ozone Satellite Homogenized (SWOOSH) dataset, which is a merged record of stratospheric ozone and water vapor measurements taken by a number of limb sounding and solar occultation satellites over the period from 1984 to 2018. Its primary product is a monthly mean zonal-mean gridded dataset (2.5° from 89°S to 89°N) containing ozone and water vapor data from the SAGE-II/III, UARS HALOE, UARS MLS, and Aura MLS instruments. The vertical pressure range of the water vapor data is 316–1 hPa (31 levels). For more information, see Davis et al.<sup>89</sup>. Another monthly water vapor data over the period from 1980 to 2017 are taken from the state-of-the-art atmospheric reanalysis, the MERRA-2, which was developed by the NASA Global Modeling and Assimilation Office (GMAO) and is described in Gelaro et al.<sup>90</sup>. The underlying atmospheric general circulation model (AGCM) is the GEOS-5 atmospheric model including the dynamical core. Its horizontal grid is a cubed sphere, with an approximate grid spacing of 0.5° in latitude and 0.625° in longitude, with 72 hybrid-eta levels from the surface to 0.01 hPa. Other meteorological values come from MERRA-2.

## Indices introduction

Following Dessler et al.<sup>24</sup>, the QBO index used in this work is normalized zonal-mean zonal wind along the equator at 50 hPa. The easterly QBO phase (EQBO) is defined as the deseasonalised monthly zonal-mean zonal wind  $\leq -2 \text{ m s}^{-1}$ , and the westerly QBO phase (WQBO) is defined as the deseasonalised monthly zonal-mean zonal wind  $\geq 2 \text{ m s}^{-1}$ <sup>91</sup>. The monthly NINO3.4 and Modoki indices (hereafter EMI) are used to represent monthly characteristics of canonical ENSO events and ENSO Modoki events,

respectively. The NINO3.4 index is defined as the area-mean SSTA over the region (5°N–5°S, 120°W–170°W).

The EMI was defined as follows (Ashok et al.<sup>92</sup>):

$$\text{EMI} = [\text{SSTA}]_C - 0.5 \times [\text{SSTA}]_E - 0.5 \times [\text{SSTA}]_W \quad (1)$$

Terms in the formula represent the area-mean SSTA.  $[\text{SSTA}]_C$  is the mean over the central Pacific region (10°S–10°N, 165°E–140°W),  $[\text{SSTA}]_E$  is over the eastern Pacific region (15°S–5°N, 110°W–70°W), and  $[\text{SSTA}]_W$  is over the western Pacific region (10°S–20°N, 125°E–145°E). SST data are obtained from the Met Office Hadley Center SST (HADSST) dataset.

## WACCM4

WACCM4 is part of the Community Earth System Model (CESM) framework developed by the National Center for Atmos.<sup>93</sup>. In this study, we use version CESM1.0.6. WACCM4 also encompasses the Community Atmospheric Model version 4 (CAM4), and as such includes all of its physical parameterizations<sup>94</sup>. This improved version of WACCM uses a coupled system made up of four components, namely atmosphere, ocean<sup>95</sup>, land, and sea ice<sup>96</sup>. WACCM4 uses a finite-volume dynamical core, with 66 vertical levels extending from the ground to  $5.1 \times 10^{-6}$  hPa (~145 km geometric altitude), and a vertical resolution of 1.1–1.4 km in the tropical tropopause layer and the lower stratosphere (located below a height of 30 km). The simulations presented in this paper are performed at a horizontal resolution of  $1.9^\circ \times 2.5^\circ$ , and include interactive tropospheric and stratospheric chemistry<sup>97</sup>. More details about WACCM4 are available in Marsh et al.<sup>98</sup>. To obtain a longer period data of water vapor, a historical run from 1955 to 2005 is performed using WACCM4. SST based on the HadISST dataset; surface emissions obtained from the

RCP45 emissions scenario developed by CMIP5; spectrally resolved solar variability; volcanic aerosols (from the SPARC CCMVal REF-B2 scenario recommendations); for this kind of experiment, the QBO is forced like ENSO forcing, ENSO would be set by SST and QBO is set by zonal wind.

## DATA AVAILABILITY

We acknowledge datasets from the SWOOSH and MERRA-2. The SWOOSH data analyzed during the current study are publicly available at <https://www.esrl.noaa.gov/csd/groups/csd8/swoosh>, and the MERRA-2 analyzed during the current study is publicly available at [https://gmao.gsfc.nasa.gov/reanalysis/MERRA-2/data\\_access](https://gmao.gsfc.nasa.gov/reanalysis/MERRA-2/data_access). The NINO3.4 index is available at <http://www.cpc.noa.gov/data/indices/>. SST data are obtained from the Met Office Hadley Center SST (HADSST) dataset: [www.metoffice.gov.uk/hadobs/index.html](http://www.metoffice.gov.uk/hadobs/index.html). The WACCM4 data analyzed in the current study are available at <https://zenodo.org/record/3911397#.XvhXy6iHrIU>.

## CODE AVAILABILITY

NCAR Command Language (NCL) computer code was used for data processing and analyses. Computer codes are available from the author upon reasonable requests.

Received: 14 February 2020; Accepted: 5 August 2020;

Published online: 03 September 2020

## REFERENCES

- Joshi, M. M., Charlton, A. J. & Scaife, A. A. On the influence of stratospheric water vapor changes on the tropospheric circulation. *Geophys. Res. Lett.* **33**, L09806 (2006).
- Forster, P. M. F. & Shine, K. Assessing the climate impact of trends in stratospheric water vapor. *Geophys. Res. Lett.* **29**, 10-11–10-14 (2002).
- Stenke, A. & Grewe, V. Simulation of stratospheric water vapor trends: impact on stratospheric ozone chemistry. *Atmos. Chem. Phys.* **5**, 1257–1272 (2005).
- Wang, W., Matthes, K., Omrani, N.-E. & Latif, M. Decadal variability of tropical tropopause temperature and its relationship to the Pacific Decadal Oscillation. *Sci. Rep.* **6**, 29537 (2016).
- Zhao, X., Sheng, Z., Li, J., Yu, H. & Wei, K. Determination of the “wave turbopause” using a numerical differentiation method. *J. Geophys. Res. Atmos.* **124**, 10592–10607 (2019).
- Solomon, S. et al. Contributions of stratospheric water vapor to decadal changes in the rate of global warming. *Science* **327**, 1219–1223 (2010).
- Joshi, M., Webb, M., Maycock, A. & Collins, M. Stratospheric water vapour and high climate sensitivity in a version of the HadSM3 climate model. *Atmos. Chem. Phys.* **10**, 7161–7167 (2010).
- Le Texier, H., Solomon, S. & Garcia, R. The role of molecular hydrogen and methane oxidation in the water vapour budget of the stratosphere. *Q. J. R. Meteorol. Soc.* **114**, 281–295 (1988).
- Brasseur, G. P. & Solomon, S. *Aeronomy of The Middle Atmosphere: Chemistry and Physics of The Stratosphere and Mesosphere*. Vol. 32 (Springer Science & Business Media, 2006).
- Tian, W., Chipperfield, M. P., Gray, L. J. & Zawodny, J. M. Quasi-biennial oscillation and tracer distributions in a coupled chemistry-climate model. *J. Geophys. Res. Atmos.* **111**, D20301 (2006).
- Randel, W. J. & Jensen, E. J. Physical processes in the tropical tropopause layer and their roles in a changing climate. *Nat. Geosci.* **6**, 169 (2013).
- Brewer, A. Evidence for a world circulation provided by the measurements of helium and water vapour distribution in the stratosphere. *Q. J. R. Meteorol. Soc.* **75**, 351–363 (1949).
- Xie, F. et al. The key role of background sea surface temperature over the cold tongue in asymmetric responses of the Arctic stratosphere to El Niño–Southern Oscillation. *Environ. Res. Lett.* **13**, 114007 (2018).
- Hurst, D. F. et al. Stratospheric water vapor trends over Boulder, Colorado: analysis of the 30 year Boulder record. *J. Geophys. Res. Atmos.* **116**, D02306 (2011).
- Hu, D., Tian, W., Xie, F., Wang, C. & Zhang, J. Impacts of stratospheric ozone depletion and recovery on wave propagation in the boreal winter stratosphere. *J. Geophys. Res. Atmos.* **120**, 8299–8317 (2015).
- Joshi, M. M. & Shine, K. P. A GCM study of volcanic eruptions as a cause of increased stratospheric water vapor. *J. Clim.* **16**, 3525–3534 (2003).
- Randel, W. J., Wu, F., Russell, J. M. III, Roche, A. & Waters, J. W. Seasonal cycles and QBO variations in stratospheric CH<sub>4</sub> and H<sub>2</sub>O observed in UARS HALOE data. *J. Atmos. Sci.* **55**, 163–185 (1998).
- Scaife, A. A., Butchart, N., Jackson, D. R. & Swinbank, R. Can changes in ENSO activity help to explain increasing stratospheric water vapor? *Geophys. Res. Lett.* **30**, 1880 (2003).
- Fueglistaler, S., Bonazzola, M., Haynes, P. & Peter, T. Stratospheric water vapor predicted from the Lagrangian temperature history of air entering the stratosphere in the tropics. *J. Geophys. Res. Atmos.* **110**, D08107 (2005).
- Fueglistaler, S. & Haynes, P. Control of interannual and longer-term variability of stratospheric water vapor. *J. Geophys. Res. Atmos.* **110**, D24108 (2005).
- Rosenlof, K. H. & Reid, G. C. Trends in the temperature and water vapor content of the tropical lower stratosphere: sea surface connection. *J. Geophys. Res. Atmos.* **113**, D06107 (2008).
- Schoeberl, M. & Dessler, A. Dehydration of the stratosphere. *Atmos. Chem. Phys.* **11**, 8433–8446 (2011).
- Grise, K. M. & Thompson, D. W. Equatorial planetary waves and their signature in atmospheric variability. *J. Atmos. Sci.* **69**, 857–874 (2012).
- Dessler, A., Schoeberl, M., Wang, T., Davis, S. & Rosenlof, K. Stratospheric water vapor feedback. *Proc. Natl Acad. Sci. USA* **110**, 18087–18091 (2013).
- Wang, W., Shangquan, M., Tian, W., Schmidt, T. & Ding, A. Large uncertainties in estimation of tropical tropopause temperature variabilities due to model vertical resolution. *Geophys. Res. Lett.* **46**, 10043–10052 (2019).
- Wang, W. et al. Solar impacts on decadal variability of tropopause temperature and lower stratospheric (LS) water vapour: a mechanism through ocean-atmosphere coupling. *Clim. Dyn.* **52**, 5585–5604 (2019).
- Gettelman, A. et al. Radiation balance of the tropical tropopause layer. *J. Geophys. Res. Atmos.* **109**, D07103 (2004).
- Fueglistaler, S. et al. Tropical tropopause layer. *Rev. Geophys.* **47**, RG1004 (2009).
- Yulaeva, E., Holton, J. R. & Wallace, J. M. J. O. T. A. S. On the cause of the annual cycle in tropical lower-stratospheric temperatures. *J. Atmos. Sci.* **51**, 169–174 (1994).
- Gettelman, A. A climatology of the tropical tropopause layer. *J. Meteorol. Soc. Jpn. Ser. II* **80**, 911–924 (2002).
- Son, S. W., Tandon, N. F. & Polvani, L. M. The fine-scale structure of the global tropopause derived from COSMIC GPS radio occultation measurements. *J. Geophys. Res. Atmos.* **116**, D20113 (2011).
- Birner, T. & Bönsch, H. Residual circulation trajectories and transit times into the extratropical lowermost stratosphere. *Atmos. Chem. Phys.* **11**, 817–827 (2011).
- Holton, J. R. et al. Stratosphere-troposphere exchange. *Rev. Geophys.* **33**, 403–439 (1995).
- Wang, L. & Waugh, D. W. Seasonality in future tropical lower stratospheric temperature trends. *J. Geophys. Res. Atmos.* **120**, 980–991 (2015).
- Xia, Y., Huang, Y., Hu, Y. & Yang, J. Impacts of tropical tropopause warming on the stratospheric water vapor. *Clim. Dyn.* **53**, 3409–3418 (2019).
- Lei, D., Jin, L., Zhu, Z. & Gao, M. Advances in the study of water vapor vertical transport into stratosphere by deep convections. *J. Nanjing Univ. Inf. Sci. Technol.* **4**, 241 (2012).
- Herman, R. L. et al. Enhanced stratospheric water vapor over the summertime continental United States and the role of overshooting convection. *Atmos. Chem. Phys.* **17**, 6113 (2017).
- Dong, W., Lin, Y., Zhang, M. & Huang, X. J. G. R. L. Footprint of tropical mesoscale convective system variability on stratospheric water vapor. *Geophys. Res. Lett.* **47**, <https://doi.org/10.1029/2019GL086320> (2020).
- Highwood, E. & Hoskins, B. The tropical tropopause. *Q. J. R. Meteorol. Soc.* **124**, 1579–1604 (1998).
- He, Y., Sheng, Z. & He, M. Spectral analysis of gravity waves from near space high-resolution balloon data in Northwest China. *Atmosphere* **11**, 133 (2020).
- Calvo, N., Giorgetta, M. A., Garcia-Herrera, R. & Manzini, E. Nonlinearity of the combined warm ENSO and QBO effects on the Northern Hemisphere polar vortex in MAECHAM5 simulations. *J. Geophys. Res. Atmos.* **114**, D13109 (2009).
- Son, S. W., Lim, Y., Yoo, C., Hendon, H. & Kim, J. Stratospheric control of Madden-Julian Oscillation. *J. Clim.* **30**, 1909–1922 (2017).
- Garcia-Herrera, R., Calvo, N., Garcia, R. & Giorgetta, M. Propagation of ENSO temperature signals into the middle atmosphere: A comparison of two general circulation models and ERA-40 reanalysis data. *J. Geophys. Res. Atmos.* **111**, D06101 (2006).
- Free, M. & Seidel, D. J. Observed El Niño–Southern Oscillation temperature signal in the stratosphere. *J. Geophys. Res. Atmos.* **114**, D23108 (2009).
- Randel, W. J., Garcia, R. R., Calvo, N. & Marsh, D. ENSO influence on zonal mean temperature and ozone in the tropical lower stratosphere. *Geophys. Res. Lett.* **36**, L15822 (2009).
- Calvo, N., Garcia, R., Randel, W. & Marsh, D. Dynamical mechanism for the increase in tropical upwelling in the lowermost tropical stratosphere during warm ENSO events. *J. Atmos. Sci.* **67**, 2331–2340 (2010).
- Gettelman, A. et al. El Niño as a natural experiment for studying the tropical tropopause region. *J. Clim.* **14**, 3375–3392 (2001).
- Geller, M. A., Zhou, X. & Zhang, M. Simulations of the interannual variability of stratospheric water vapor. *J. Atmos. Sci.* **59**, 1076–1085 (2002).
- Hatsushika, H. & Yamazaki, K. Stratospheric drain over Indonesia and dehydration within the tropical tropopause layer diagnosed by air parcel trajectories. *J. Geophys. Res. Atmos.* **108**, 4610 (2003).

50. Xie, F., Li, J., Tian, W., Feng, J. & Huo, Y. Signals of El Niño Modoki in the tropical tropopause layer and stratosphere. *Atmos. Chem. Phys.* **12**, 5259–5273 (2012).
51. Camp, C. & Tung, K. K. Stratospheric polar warming by ENSO in winter: a statistical study. *Geophys. Res. Lett.* **34**, L04809 (2007).
52. Garfinkel, C. I. & Hartmann, D. L. Effects of the El Niño–Southern Oscillation and the quasi-biennial oscillation on polar temperatures in the stratosphere. *J. Geophys. Res. Atmos.* **112**, D19112 (2007).
53. Garfinkel, C. & Hartmann, D. Different ENSO teleconnections and their effects on the stratospheric polar vortex. *J. Geophys. Res. Atmos.* **113**, D18114 (2008).
54. Ren, R.-C., Cai, M., Xiang, C. & Wu, G. Observational evidence of the delayed response of stratospheric polar vortex variability to ENSO SST anomalies. *Clim. Dyn.* **38**, 1345–1358 (2012).
55. Li, T. et al. Southern hemisphere summer mesopause responses to El Niño–Southern oscillation. *J. Clim.* **29**, 6319–6328 (2016).
56. Sassi, F., Kinnison, D., Boville, B., Garcia, R. & Roble, R. Effect of El Niño–Southern Oscillation on the dynamical, thermal, and chemical structure of the middle atmosphere. *J. Geophys. Res. Atmos.* **109**, D17108 (2004).
57. Manzini, E., Giorgetta, M., Esch, M., Kornblueh, L. & Roeckner, E. The influence of sea surface temperatures on the northern winter stratosphere: Ensemble simulations with the MAECHAM5 model. *J. Clim.* **19**, 3863–3881 (2006).
58. Taguchi, M. & Hartmann, D. L. Increased occurrence of stratospheric sudden warmings during El Niño as simulated by WACCM. *J. Clim.* **19**, 324–332 (2006).
59. Garfinkel, C. I., Hurwitz, M. M., Oman, L. D. & Waugh, D. W. Contrasting effects of Central Pacific and Eastern Pacific El Niño on stratospheric water vapor. *Geophys. Res. Lett.* **40**, 4115–4120 (2013).
60. Rao, J. & Ren, R. Asymmetry and nonlinearity of the influence of ENSO on the northern winter stratosphere: 2. Model study with WACCM. *J. Geophys. Res. Atmos.* **121**, 9017–9032 (2016).
61. Xie, F. et al. Effect of the Indo-Pacific warm pool on lower-stratospheric water vapor and comparison with the effect of ENSO. *J. Clim.* **31**, 929–943 (2018).
62. Mitchell, D., Gray, L. & Charlton-Perez, A. The structure and evolution of the stratospheric vortex in response to natural forcings. *J. Geophys. Res. Atmos.* **116**, D15110 (2011).
63. Iza, M. & Calvo, N. Role of stratospheric sudden warmings on the response to central Pacific El Niño. *Geophys. Res. Lett.* **42**, 2482–2489 (2015).
64. Zhang, J., Tian, W., Wang, Z., Xie, F. & Wang, F. The influence of ENSO on northern midlatitude ozone during the winter to spring transition. *J. Clim.* **28**, 4774–4793 (2015).
65. Iza, M., Calvo, N. & Manzini, E. The stratospheric pathway of La Niña. *J. Clim.* **29**, 8899–8914 (2016).
66. Ashok, K. & Yamagata, T. Climate change: the El Niño with a difference. *Nature* **461**, 481 (2009).
67. Yeh, S.-W. et al. El Niño in a changing climate. *Nature* **461**, 511 (2009).
68. Hegyi, B. M. & Deng, Y. A dynamical fingerprint of tropical Pacific sea surface temperatures on the decadal-scale variability of cool-season Arctic precipitation. *J. Geophys. Res. Atmos.* **116**, D20121 (2011).
69. Hurwitz, M., Newman, P., Oman, L. & Molod, A. Response of the Antarctic stratosphere to two types of El Niño events. *J. Atmos. Sci.* **68**, 812–822 (2011).
70. Hurwitz, M. M., Newman, P. A. & Garfinkel, C. I. The Arctic vortex in March 2011: a dynamical perspective. *Atmos. Chem. Phys.* **11**, 11447–11453 (2011).
71. Zubiaurre, I. & Calvo, N. The El Niño–Southern Oscillation (ENSO) Modoki signal in the stratosphere. *J. Geophys. Res. Atmos.* **117**, D04104 (2012).
72. Sung, M.-K., Kim, B.-M. & An, S.-I. Altered atmospheric responses to eastern Pacific and central Pacific El Niños over the North Atlantic region due to stratospheric interference. *Clim. Dyn.* **42**, 159–170 (2014).
73. Xie, F., Li, J., Tian, W., Zhang, J. & Sun, C. The relative impacts of El Niño Modoki, canonical El Niño, and QBO on tropical ozone changes since the 1980s. *Environ. Res. Lett.* **9**, 064020 (2014).
74. Xie, F., Li, J., Tian, W., Zhang, J. & Shu, J. The impacts of two types of El Niño on global ozone variations in the last three decades. *Adv. Atmos. Sci.* **31**, 1113–1126 (2014).
75. Lu, J. et al. Interannual variations in lower stratospheric ozone during the period 1984–2016. *J. Geophys. Res. Atmos.* **124**, 8225–8241 (2019).
76. Reid, G. C. & Gage, K. S. Interannual variations in the height of the tropical tropopause. *J. Geophys. Res. Atmos.* **90**, 5629–5635 (1985).
77. Ding, Q. & Fu, Q. A warming tropical central Pacific dries the lower stratosphere. *Clim. Dyn.* **50**, 2813–2827 (2018).
78. Shanguan, M. Variability of temperature and ozone in the upper troposphere and lower stratosphere from multi-satellite observations and reanalysis data. *Atmos. Chem. Phys.* **19**, 6659–6679 (2019).
79. Reed, R. A tentative model of the 26-month oscillation in tropical latitudes. *Q. J. R. Meteorol. Soc.* **90**, 441–466 (1964).
80. Randel, W. J., Wu, F., Oltmans, S. J., Rosenlof, K. & Nedoluha, G. E. Interannual changes of stratospheric water vapor and correlations with tropical tropopause temperatures. *J. Atmos. Sci.* **61**, 2133–2148 (2004).
81. Wallace, J. M., Panetta, R. L. & Estberg, J. Representation of the equatorial stratospheric quasi-biennial oscillation in EOF phase space. *J. Atmos. Sci.* **50**, 1751–1762 (1993).
82. Kumar, V. et al. Impact of quasi-biennial oscillation on the inter-annual variability of the tropopause height and temperature in the tropics: a study using COSMIC/FORMOSAT-3 observations. *Atmos. Res.* **139**, 62–70 (2014).
83. Rosenlof, K. H. How water enters the stratosphere. *Science* **302**, 1691–1692 (2003).
84. Newell, R. E. & Gould-Stewart, S. A stratospheric fountain? *J. Atmos. Sci.* **38**, 2789–2796 (1981).
85. Ding, Q. & Steig, E. J. Temperature change on the Antarctic Peninsula linked to the tropical Pacific. *J. Clim.* **26**, 7570–7585 (2013).
86. Garfinkel, C., Hurwitz, M., Waugh, D. & Butler, A. Are the teleconnections of Central Pacific and Eastern Pacific El Niño distinct in boreal wintertime? *Clim. Dyn.* **41**, 1835–1852 (2013).
87. Wang, L. et al. Prediction of northern summer low-frequency circulation using a high-order vector auto-regressive model. *Clim. Dyn.* **46**, 693–709 (2016).
88. Xie, F., Li, J., Tian, W., Li, Y. & Feng, J. Indo-Pacific warm pool area expansion, modoki activity, and tropical cold-point tropopause temperature variations. *Sci. Rep.* **4**, 4552 (2014).
89. Davis, S. M. et al. The Stratospheric Water and Ozone Satellite Homogenized (SWOOSH) database: a long-term database for climate studies. *Earth Syst. Sci. Data* **8**, 461 (2016).
90. Gelaro, R. et al. The modern-era retrospective analysis for research and applications, version 2 (MERRA-2). *J. Clim.* **30**, 5419–5454 (2017).
91. Garfinkel, C. I. & Hartmann, D. J. J. O. G. R. A. Influence of the quasi-biennial oscillation on the North Pacific and El Niño teleconnections. *J. Geophys. Res. Atmos.* **115**, D20116 (2010).
92. Ashok, K., Behera, S. K., Rao, S. A., Weng, H. & Yamagata, T. El Niño Modoki and its possible teleconnection. *J. Geophys. Res. Oceans* **112**, C11007 (2007).
93. Hurrell, J. W. et al. The community earth system model: a framework for collaborative research. *Bull. Am. Meteor. Soc.* **94**, 1339–1360 (2013).
94. Neale, R. B. et al. The mean climate of the Community Atmosphere Model (CAM4) in forced SST and fully coupled experiments. *J. Clim.* **26**, 5150–5168 (2013).
95. Danabasoglu, G. et al. The CCSM4 ocean component. *J. Clim.* **25**, 1361–1389 (2012).
96. Holland, M. M., Bailey, D. A., Briegleb, B. P., Light, B. & Hunke, E. Improved sea ice shortwave radiation physics in CCSM4: The impact of melt ponds and aerosols on Arctic sea ice. *J. Clim.* **25**, 1413–1430 (2012).
97. Garcia, R., Marsh, D., Kinnison, D., Boville, B. & Sassi, F. Simulation of secular trends in the middle atmosphere, 1950–2003. *J. Geophys. Res. Atmos.* **112**, D09301 (2007).
98. Marsh, D. R. et al. Climate change from 1850 to 2005 simulated in CESM1 (WACCM). *J. Clim.* **26**, 7372–7391 (2013).

## ACKNOWLEDGEMENTS

This work was supported by strategic priority research program of the Chinese Academy of Science (XDA17010106) and the National Natural Science Foundation of China (41975047, 41875046, and 41705022). SST dataset is obtained from the UK Met Office Hadley Centre. We thank NCAR for providing the WACCM4 model (<https://www2.cesm.ucar.edu/models/current>).

## AUTHOR CONTRIBUTIONS

J.L. and F.X. designed the study, analyzed the results, and led the writing of this work. J.L. and F.X. discussed the main results section and analyzed WACCM4 modeling simulations. F.X. designed and conducted WACCM4 simulations. C.S., J.L., J.Z., H.T., Q.C., and J.L. contributed in discussion of the manuscript. All co-authors reviewed the manuscript.

## COMPETING INTERESTS

The authors declare no competing interests.

## ADDITIONAL INFORMATION

**Correspondence** and requests for materials should be addressed to F.X.

**Reprints and permission information** is available at <http://www.nature.com/reprints>

**Publisher's note** Springer Nature remains neutral with regard to jurisdictional claims in published maps and institutional affiliations.



**Open Access** This article is licensed under a Creative Commons Attribution 4.0 International License, which permits use, sharing, adaptation, distribution and reproduction in any medium or format, as long as you give appropriate credit to the original author(s) and the source, provide a link to the Creative

Commons license, and indicate if changes were made. The images or other third party material in this article are included in the article's Creative Commons license, unless indicated otherwise in a credit line to the material. If material is not included in the article's Creative Commons license and your intended use is not permitted by statutory regulation or exceeds the permitted use, you will need to obtain permission directly from the copyright holder. To view a copy of this license, visit <http://creativecommons.org/licenses/by/4.0/>.

© The Author(s) 2020